21, rue d'Artois, F-75008 PARIS
http : //www.cigre.org

CIGRE US National Committee
2022 Grid of the Future Symposium

Demonstration of a Self-healing Power System Concept using Manufacturer Specific Inverter Models

E. SILVA[1], M.E. ROPP[2], O. LAVROVA[1]
[2]Sandia National Laboratories, [1]New Mexico State University
USA

SUMMARY

Self-healing power systems can provide significant resilience benefits. However, most self-healing power systems concepts rely on data sharing via communications that may be cost-prohibitive or that could become unreliable during contingency events. Self-healing, or self-assembly, via local measurements only would have some significant advantages, if sufficient performance can be achieved. This paper presents simulations demonstrating the use of a specific set of techniques to achieve self-assembly and self-healing in the IEEE 13-bus distribution test circuit, using only local measurements, when energized only by distributed inverter-based resources. Black start, fault isolation, and system restoration are demonstrated. The inverter-based resources are represented by manufacturer-specific code-based models. The results indicate that the performance of the local-measurements-only system can be comparable to other techniques, in the cases tested.

KEYWORDS

Self-Healing Power Systems; Microgrids; Intentional Island Power Systems; Distributed Energy Resources; Black Start; Fault Isolation; System Restoration; Inverter-Based Resources; IEEE 13-bus Distribution Test Circuit

eli01@nmsu.edu

INTRODUCTION

A self-healing power system (SHePS) has the ability to automatically detect when it is not operating properly and restore as much of the system as possible to normal operation [1]. A SHePS must be able to perform several critical power system functions, including a) protection, which includes detection of faults and isolation of faulted parts of the system; and b) restoration of service, in which all of the undamaged parts of the system are re-energized. SHePS have been extensively reported on in the literature [2-6], and Fault Location, Isolation and System Restoration (FLISR)-type SHePS [7], such as those described in [8] and [9], are commercially available today.

Nearly all of today's SHePS concepts rely on data sharing via high-speed networked communications [10]. Communications improve performance under "blue-sky" conditions and can offer many enhancements in resiliency situations, but a) the communications systems are expensive, often to the point of rendering projects unfeasible; and b) communications can become unreliable during "black-sky" events, blinding protection and control algorithms to parts of the power system that may themselves be damaged or undamaged. Maurer et.al. wrote in 2012: "Communications is the Achilles' Heal *(sic)* of any self-healing system. No matter what type of self-healing system you select—centralized, substation-based, or distributed intelligence—that fact is still true." [11] Concepts based on data sharing also often struggle with scalability and cybersecurity challenges. There is thus a need for SHePS technologies that rely on *local measurements only*, and that support ad-hoc networking of microgrids.

However, when one is limited to local measurements only, two additional challenges appear. The first is that with SHePS energized entirely by distributed inverter-based resources (IBRs) including solid-state transformers, time-overcurrent protection, which is the most-used protection tool in distribution systems [12], becomes ineffective due to the fault current limitations of the power electronics [13]. Directional elements would generally be the next tool used, followed by distance relays [14], but these too become unreliable with geographically-distributed IBRs. When a fault occurs in a SHePS energized only by IBRs, typically a widespread undervoltage occurs because the IBRs reach their current limits and cease voltage regulation. This undervoltage often has a low spatial gradient, rendering coordination of undervoltage-based protection difficult. Thus, in a SHePS of this type, it is not difficult to detect the *existence* of a fault, but it is difficult to ascertain the fault's *location*.

The second challenge arises because today's restoration procedures are also designed around a centralized system architecture energized by rotating machines [15]. System restoration is a complex process that involves coordinating black-start resources, identifying critical paths, estimating surge loads during re-energization, and understanding the dynamics of the system at each step of the restoration process [16]. It is widely recognized that distributed resources can assist with system restoration, but most proposed techniques for achieving this still rely on centralized communication and control [16,17].

PROPOSED SOLUTION

Investigators at Sandia National Laboratories and New Mexico State University have been collaborating on a project called "SHAZAM" ("Self-Healing Adaptive Zeta-Alpha Microgrids"), in which a set of tools that facilitates creating self-assembling SHePS energized by distributed IBRs, using local measurements only [18,19,20], has been developed. The SHAZAM concept utilizes line relays, which sectionalize the system's main conductors, and load relays, which may be implemented in "smart meters" and which contain a number of automatic load-shedding and reconnection functions. For example, Figure 1 shows a one-line

diagram of the IEEE 13-bus distribution test circuit [21] configured to operate as three separate self-networking microgrid using this SHePS concept. The red blocks are closed relays. Each load has a load relay, and there are ten line relays, R1 through R10. This system has a microgrid isolation device, which is shown as green indicating that it is open and this system is off-grid.

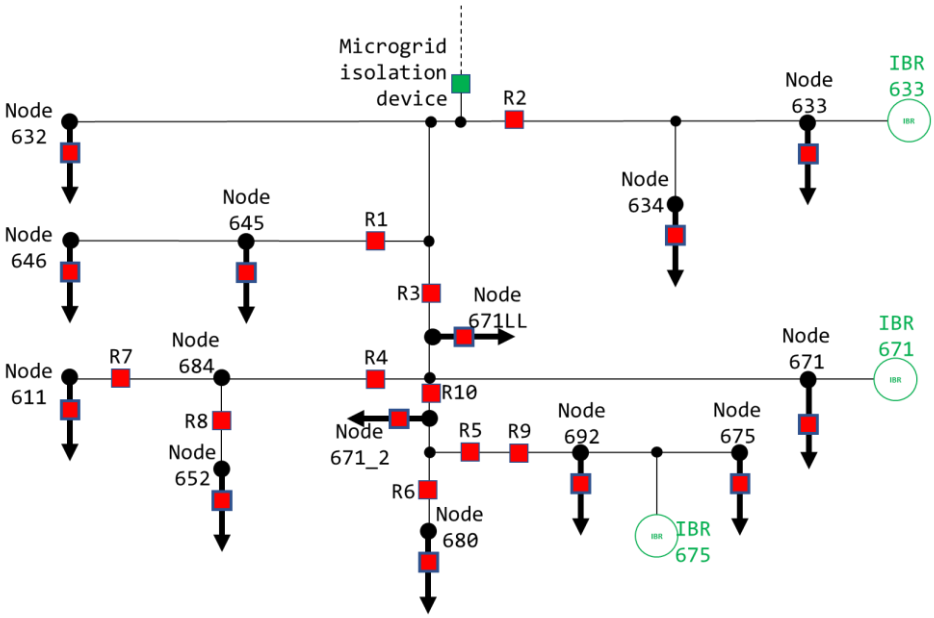

Figure 1. IEEE 13-bus system configured as three microgrids, each with a grid-forming inverter-based resource.

The system loads are first separated into priority categories. For this example, three categories, A, B and C, are used. Group A is the highest priority group and will be shed last, if at all, and group C is lowest priority and will be shed first. Load shedding is achieved via time-underfrequency and time-undervoltage. The time to trip, t_{open}, is given by

$$t_{open} = t_{fixed,o} + t_{rand,o} \quad (1)$$

where $t_{rand,o}$ is a randomly-generated time delay, and $t_{fixed,o}$ is a function of voltage and assigned load group. The values of $t_{fixed,o}$, and the ranges of t_{open}, are shown in Figure 2. The line relays use a time-undervoltage logic similar to that shown in Figure 2, time-coordinated with the load relays.

When either a fault or an overload occurs, the IBRs will reach their current limits and will allow the voltage to fall, leading to a systemwide undervoltage event. During such an event, the time-undervoltage logic will first shed load group C, as shown in Figure 2. If the undervoltage persists, then load group B is shed, followed by group A. If all load shedding has been exhausted and the undervoltage still persists, then the undervoltage is likely due to a fault, and at this point all line relays open, disassembling the system. The only portions of the system that remain energized are small "core" microgrids centered around each grid-forming IBR. Self-reassembly of the system then begins. Any line relay that sees in-range voltage on one side only is allowed to reclose after time t_{close} has elapsed, where t_{close} is defined as

$$t_{close} = t_{fixed,c} + t_{tag} + t_{rand,c} \quad (2)$$

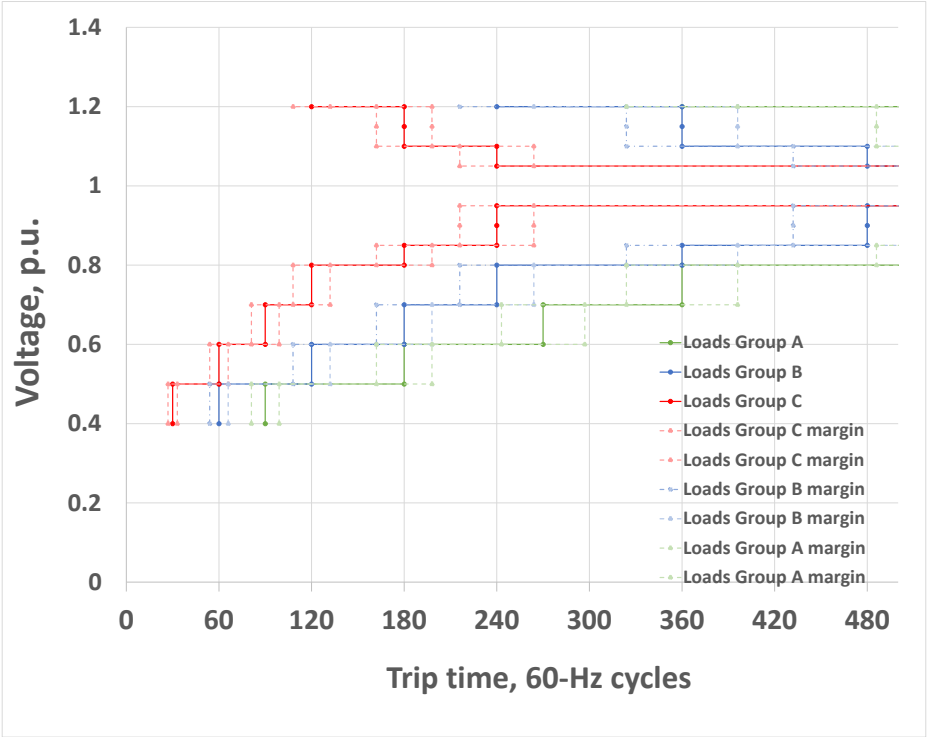

Figure 2. Time-undervoltage function used in load relays in SHAZAM, showing values of t_{fixed} (solid lines) and the limits of t_{open} (dashed lines). The function used for line relays is similar.

where $t_{fixed,c}$ is a fixed time period, t_{tag} is a time that is assigned to each line relay in such a way that no two adjacent line relays have the same value of $t_{tag,}$ and $t_{rand,c}$ is a random time interval that is much smaller than t_{tag}. If a line relay sees in-range voltage on both sides, the relay can close after two conditions are satisfied: a) a synchronization check function (IEEE function number 25 [22]) has verified that the voltages on each side of the relay are sufficiently similar in magnitude and the phase angle difference between them is sufficiently small; and b) an unintentional loop detection function has verified that closure of that relay will not create a closed loop in a system designed to be operated radially [18]. In this work, the synchronization-check function requires phase matching within 2^{o} and magnitude matching within 5%.

Each line relay also includes an undervoltage-supervised overcurrent (UVOC, or 51V) function. The UVOC function monitors the voltage and current within a time window after each load and line relay closes. If the line relay current is over a threshold *and* the voltage is lower than a threshold over the entire time window, then the line relay assumes that it has closed onto a fault, and it re-opens and locks out. This results in isolation of the fault, and if fault indicators are included on the line relays, it also provides arriving crews general information on where the fault is located. The time window must be set long enough that large motor starts do not activate the UVOC function. In this work, the current threshold used is 0.8 pu, the undervoltage threshold is 0.8 pu, and the length of the time window is 200 ms.

As the line relays close, load relays in their zones will begin to see in-range voltage, and they will begin to reclose after a time delay that is specific to each load group. It is generally desirable that not all of the load relays within a single load group reclose at the same time, so similar to the case of the line relays (Equation (2)), a random delay is included that varies each load relay's closure time by ±10% of the base reclose time assigned to that load group. The

IBRs in the microgrids all utilize the same linear power-frequency droop characteristic, so that the system frequency can be used by the load relays as an indication of available capacity. If the frequency falls too low, indicating insufficient IBR capacity, load relays will not reclose, thus avoiding an overload. Hysteresis is used on the load relay frequency function to prevent chattering (i.e., the load relays open at a frequency f_{open} and close at a frequency f_{close}, where $f_{close} > f_{open}$).

DEMONSTRATION IN EMT SIMULATION

Testing of this logic has been carried out in PSCAD using the IEEE 13 bus system which has been separated into three microgrids (Figure 1), each with an IBR. The same system configuration and loads are used in all of the simulations described below. Testing was performed with both generic and manufacturer-specific IBR models. This testing emphasized the critical importance of proper modeling of the IBRs' current-limiting functions. The generic model used here had a current limiter that did not reach full clamping of the inverter current for about 30 cycles, prior to which it allowed significantly higher current to flow. This elevated fault current is unrealistic when compared to the responses of real-world IBRs, which according to manufacturer-provided data typically limit fault current within 2 cycles or even less. This exaggerated fault current can lead to misleading results for several of the SHAZAM functions, especially UVOC, so in this paper the results shown are all obtained using a manufacturer-specific, code-based PSCAD inverter model. All of the step-up transformers used with the IBRs are delta on the inverter side and grounded-Y on the feeder side, so they provide ground-fault current.

The line relay tag assignments used in this work are shown in Table 1, and the load group assignments are given in Table 2. (The line relay and load-node numbers refer to the IEEE 13-bus system shown in Figure 1.)

Table 1: Tag values used in each line relay.

Line Relay	R1	R2	R3	R4	R5	R6	R7	R8	R9	R10
Tag Value	1	1	0	0	1	1	1	1	0	0

Table 2. Load group assignments.

Load number	632	675	680	671_2	692	611	652	645	646	671	634	671LL
Load Group	A	B	C	A	B	C	A	B	C	A	B	C

Black Start

The black-start case is shown in Figure 3. This figure shows the PSCAD model of the 13-bus system, off-grid, with the three grid-forming IBRs. The colored lines show the boundaries of the microgrids at different stages along the black-start process. At the beginning of the black-start case, all line and load relays are open, which creates a set of isolated core microgrids centered around each IBR indicated by the **red** boundaries in Figure 3. At the edge of each core microgrid is an open line relay that sees in-range voltage on one side, and 'zero' voltage on the other side. These line relays are allowed to close after their time delay t_{close} (Equation (2)) has elapsed. The line relays with a tag value of zero (Table 1) close first, expanding the microgrid boundaries to the **blue** lines in Figure 3.

Note that there is not a blue microgrid boundary near IBR 633 (the one at the top of Figure 3). That is because the line relay at the boundary of that microgrid, line relay R2, sees good voltage on one side only but it has a tag value of 1 (Table 1). Thus, it has a longer reclose delay t_{close} and does not close with the rest of the 'blue' group.

The next set of line relays then close, moving the microgrid boundaries to the **green** lines in Figure 3. All of these close due to seeing in-range voltage on one side only, except for R2, which is between microgrids 633 and 671. At this step in the process, R2 sees in-range voltage on both sides, and it closes after synchronization check and loop-prevention functions are satisfied.

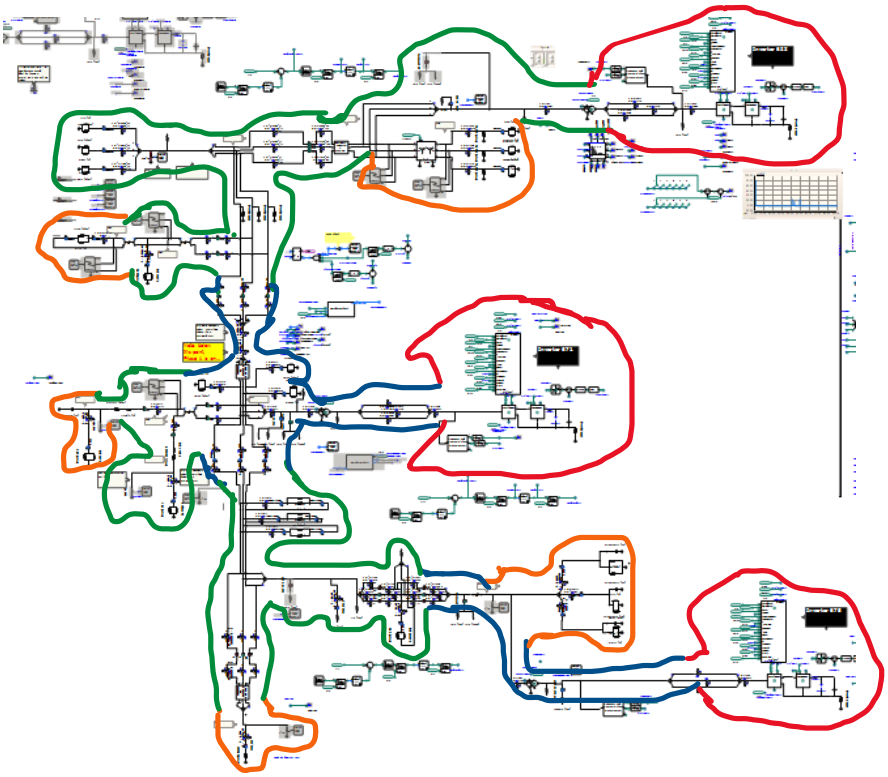

Figure 3. Diagram showing propagation of microgrid boundaries during the black-start case.

At this point, all of the line relays are closed. Load relays will begin closing according to their group-specific closure delays as soon as they are supplied with in-range voltage. In this example, the final group of load relays closes to move the microgrid boundaries to the orange lines in Figure 3. In this scenario there are sufficient resources to carry all of the loads, so the frequency does not drop below the load relay underfrequency thresholds, and in the final system state all of the loads are energized.

A-B fault at load 632

In this use case, a phase-to-phase fault occurs at node 632 at t = 15 s. When the fault occurs, the IBRs reach their current limits, the voltage collapses, and the system begins to shed load following the time-undervoltage function in Figure 2. The load-shedding process is illustrated in Figure 4. The loads marked by **red** X's, all in group C, trip within the first 1 s after the fault occurs. The undervoltage persists, so the next set of loads, marked by **blue** X's, are shed between 1 and 1.5 s post-fault. At 1.5 s post-fault, half of the line relays (R1, R4, R6, R7, and R8) unexpectedly open, possibly indicating a miscoordination. Finally, between 2 and 2.5 s post-fault, the final load group trips, marked by **orange** X's.

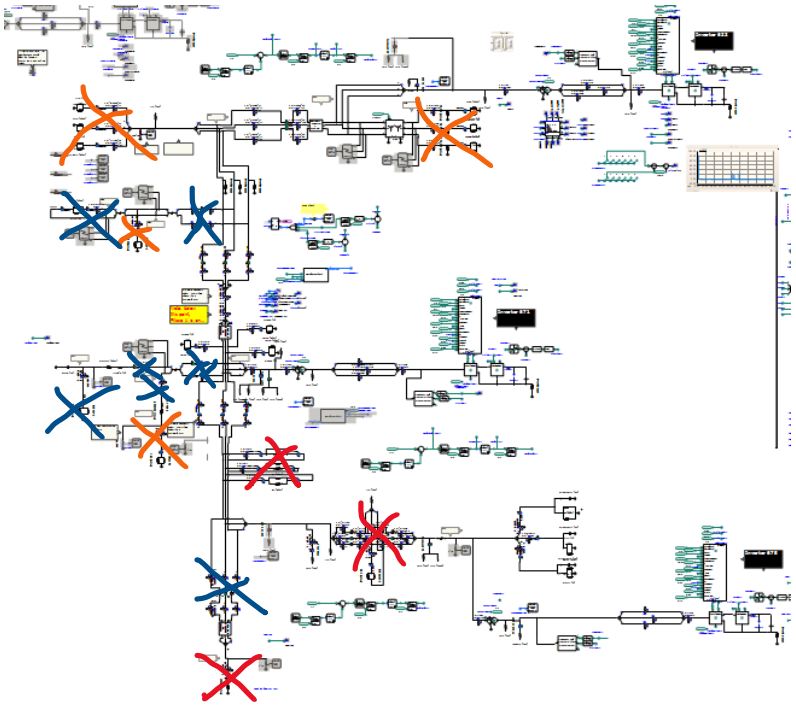

Figure 4. Load shedding following an A→B fault at node 632.

When load shedding is completed, the fault persists and thus the undervoltage persists. At that point, about 3 s post-fault, all of the remaining line relays open, forming the three 'core microgrids' whose boundaries are the **red** lines in Figure 5. Note that two of the loads, the ones closest to IBRs 671 and 675, never trip in this case; they are not in a faulted zone and are between the IBR and the first line relay, so their voltages remain high enough that the fault is cleared before they trip on undervoltage.

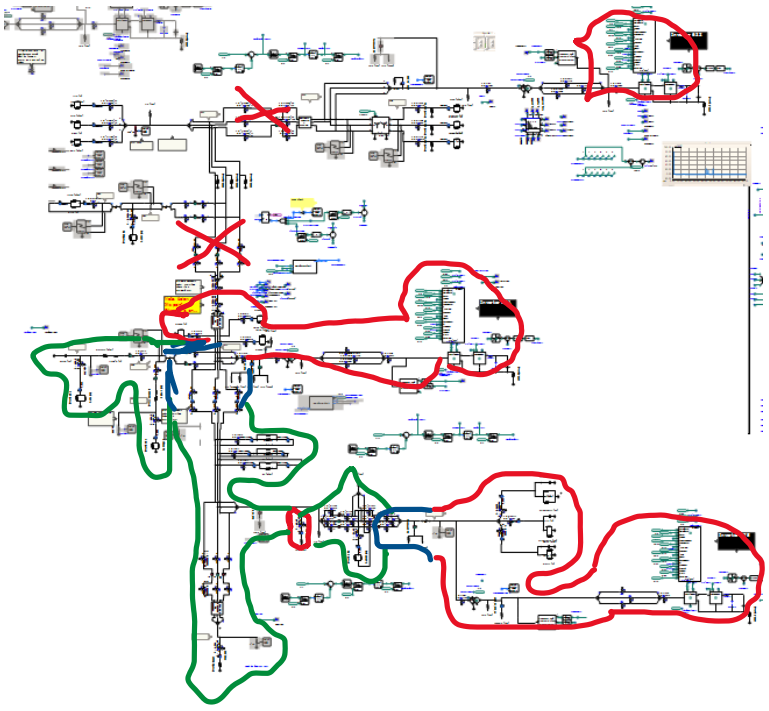

Figure 5. System reassembly following A→B fault at node 632.

The reassembly process is illustrated in Figure 5, and proceeds similarly to the black-start case. The first line-relay reclosure moves the boundaries of microgrids 671 and 675 to the **blue** boundaries, over an interval stretching from about 3.9 to 6.0 s after the fault. Also, line relay R3 closes onto the fault at 3.9 s post-fault, then re-opens and locks out on UVOC, as indicated by the red X near the center of Figure 5. Similarly, at 5.45 s post-fault, R2 recloses onto the fault, then re-opens and locks out on UVOC, indicated by the red X toward the upper left corner of Figure 5. At roughly 13 s post-fault, the system has reached its final state: microgrid 633 is operating in isolation, microgrids 671 and 675 have reconnected, the faulted zone around node 632 is isolated, and all of the loads outside of the faulted zone are being served. The load and line relay reclosing times are given in Tables 3 and 4, respectively. Load relalys 632 and 634 remain open because they are in the faulted zone.

Table 3. Load relay closing times (post-fault) for the AB fault at node 632. NT = never tripped ; RO = remains open.

Load	632	675	680	671_2	611	692	652	645	646	671	634	671LL
Closing time (s)	RO	NT	11.5	NT	13.2	6.6	9.2	2.1	1.1	NT	RO	8.7

Table 4. Line relay closing times (post-fault) for the AB fault at node 632. RO = remains open.

Line Relay	R1	R2	R3	R4	R5	R6	R7	R8	R9	R10
Closing Time (s)	RO	5.45; UVOC lockout at 5.47	3.90; UVOC lockout at 3.93	6.1	9.6	6.2	8.2	23.265s	3.9	3.9

A-G fault at load 633

In this use case, a phase A-to-ground fault occurs at node 633. IBR 633 is in the faulted zone in this case. As before, the load relays open on time-undervoltage as shown in Figure 6. First to open are the group C loads marked with **red** X's, all within 1 s post-fault. At 1.5 s post-fault, most of the line relays open (**blue** X's). The group B loads marked with **green** X's open just before 2 s post-fault, and the last group of loads to trip, all group A, are marked with orange X's and trip around 3 s post-fault. Loads 671 and 675 did not trip in this case because they are each close to an IBR, so the fault was cleared before their time-undervoltage functions timed out.

The system then self-assembles as shown in Figure 7. At first, the boundaries of the energized microgrids are the **red** lines. The first set of line relays closes, extending the boundaries to the **blue** lines, then to the **green**, and then to the **orange**. The load and line relay closure times post-fault are given in Tables 6 and 7, respectively.

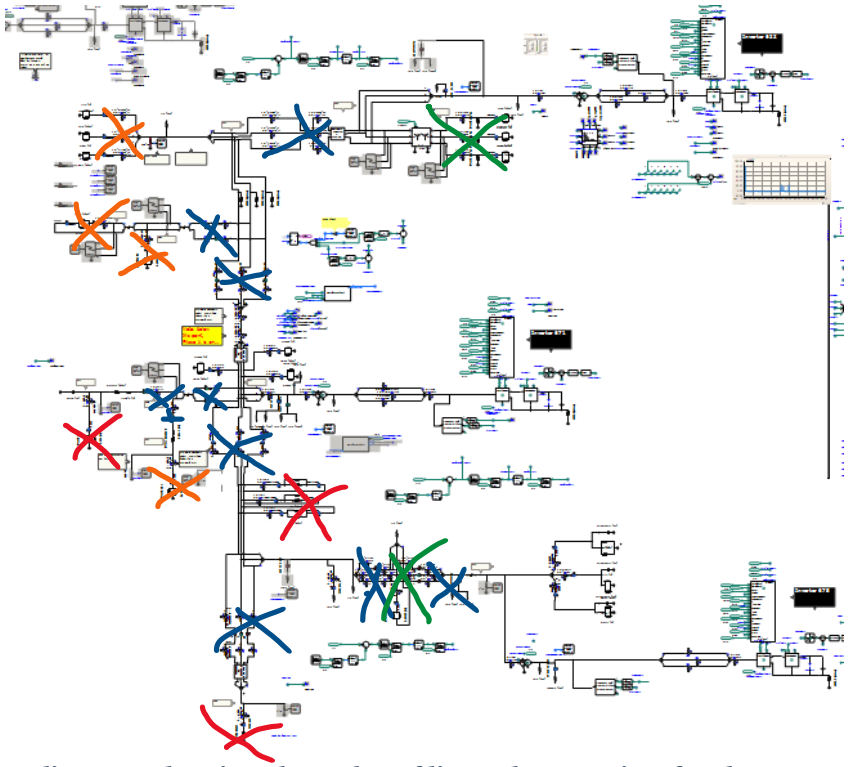

Figure 6. System diagram showing the order of line relay opening for the case of a 1LG fault at node 633.

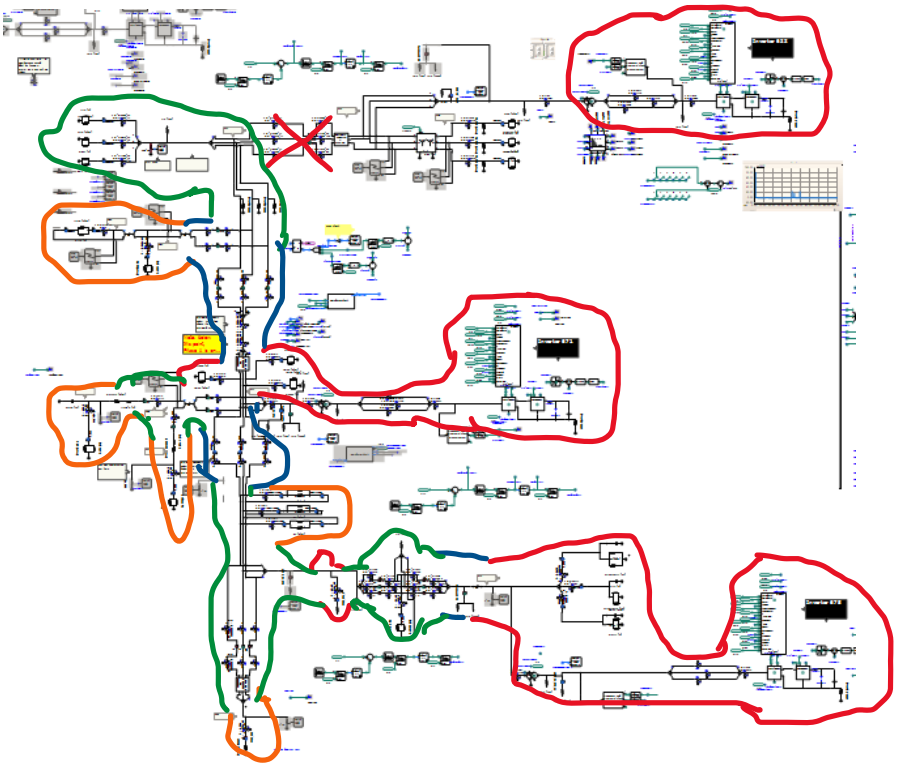

Figure 7. Reassembly of the 13-bus system after the 1LG fault at node 633.

Table 5. Load relay closing times (post-fault) for the AG fault at node 633. NT = never tripped; RO = remained open.

Load	632	675	680	671_2	611	692	652	645	646	671	634	671LL
Closing time (s)	4.7	NT	11.6	NT	11.4	6.7	7.3	9.4	11.6	NT	1.8	11.4

Table 6. Line relay reclose times (post-fault) for the AG fault at node 633.

Line Relay	R1	R2	R3	R4	R5	R6	R7	R8	R9	R10
Closing Time (s)	6.07	6.12; UVOC lockout at 6.16	3.71	3.36	7.14	6.07	5.72	5.73	3.69	3.71

CONCLUSION

This paper has demonstrated simulated self-assembly of three microgrids in the IEEE 13-bus distribution test feeder, using exclusively techniques that rely on *local measurements only*. These simulations were conducted using manufacturer-specific code-based IBR models. Three use cases, a black start case and two fault cases, are presented, and in all three cases the performance of the self-assembling or self-healing system is very good: the system reaches its new steady state in less than 14 seconds, successfully isolates faults, and successfully picks up all loads for which there is source capacity and intact source-load paths.

ACKNOWLEDGMENT

The authors gratefully acknowledge the key contributions of Raymond Byrne and Matthew Reno (Sandia National Laboratories) and Satish Ranade (New Mexico State University) to the SHAZAM concept.

This work was supported by the Laboratory Directed Research and Development program at Sandia National Laboratories, a multimission laboratory managed and operated by National Technology and Engineering Solutions of Sandia LLC, a wholly owned subsidiary of Honeywell International Inc. for the U.S. Department of Energy's National Nuclear Security Administration under contract DE-NA0003525.

This article has been authored by an employee of National Technology & Engineering Solutions of Sandia, LLC under Contract No. DE-NA0003525 with the U.S. Department of Energy (DOE). The employee owns all right, title and interest in and to the article and is solely responsible for its contents. The United States Government retains and the publisher, by accepting the article for publication, acknowledges that the United States Government retains a non-exclusive, paid-up, irrevocable, world-wide license to publish or reproduce the published form of this article or allow others to do so, for United States Government purposes. The DOE will provide public access to these results of federally sponsored research in accordance with the DOE Public Access Plan https://www.energy.gov/downloads/doe-public-access-plan.

This work was also partially supported by the NSF Grants #OIA-1757207 (NM EPSCoR), HRD-1345232 and HRD-1914635.

REFERENCES

[1] D. Ghosh, R. Sharman, H. Rao, S. Upadhyaya, "Self-Healing Systems—Survey and Synthesis", *Elsevier Decision Support Systems* **42** 2007, p. 2164-2185.

[2] Li, Z. Chen, L. Fan, P. Zhang, "Toward A Self-Healing Protection and Control System", 40th North American Power Symposium, Sept 2008.

[3] Y. Liu, R. Fan, V. Terzija, "Power System Restoration: A Literature Review From 2006 to 2016", *Journal of Modern Power Systems and Clean Energy* **4**(3), July 2016, p. 332-341.

[4] R. Campos, C. Figueroa, H. Oyarzun, J. Baeza, "Self-Healing of Electric Distribution Networks: A Review", 7th IEEE International Confernece on Computers Communications and Control (ICCCC), May 2018.

[5] M. Elgenedy, A. Massoud; S. Ahmed, "Smart grid self-healing: Functions, applications, and developments", *First IEEE Workshop on Smart Grid and Renewable Energy (SGRE)*, March 2015.

[6] S. Refaat, A. Mohamed, P. Kakosimos, "Self-Healing Control Strategy: Challenges and Opportunities for Distribution Systems in Smart Grid", 12th IEEE International Conference on Compatibility, Power electronics and Power Engineering, April 2018.

[7] J. Liu, X. Dong, X. Chen, X. Tong, X. Zhang, S. Xu, Fault Location and Service Restoration for Electrical Distribution Systems, pub. Wiley 2016, 978-1-118-95025-8.

[8] S&C Electric Intelliteam, https://www.sandc.com/en/products--services/products/intelliteam-sg-automatic-restoration-system/.

[9] SEL's "DNA", https://cms-cdn.selinc.com/assets/Literature/Publications/Case%20Studies/LCS0030_Westar%20Energy%20Case%20Study_20141103.pdf?v=20161024-215235.

[10] D. Lagos, V. Papaspiliotopoulos, G. Korres, N. Natziargyriou, "Microgrid Proection Against Internal Faults", *IEEE Power and Energy Magazine* May/June 2021, p. 20-35.

[11] L. Maurer, A. Stevens, W. Reder, "Tales From the Frontline: Keys to Successful Self-Healing Distribution Projects", *IEEE Power and Energy Magazine* **10**(2), March/April 2012, p. 100-106.

[12] L Yang, F. Xiao, H. Chen, Y. Lai, Y. Chollot, "The Experiences of Decentralized Self-Healing Grid", 8th IEEE International Conference on Advanced Power System Automation and Protection (APAP), October 2019.

[13] M. Reno, S. Brahma, A. Bidram, M. Ropp, "Influence of Inverter-Basaed Resources on Microgrid Protection (Part 1)", *IEEE Power and Energy Magazine* **19**(3), May/June 2021, p. 36-46.

[14] P. Anderson, Power System Protection, New York, NY: IEEE Press, 1999, ISBN 978-0-78-033427-4.

[15] Y. Liu, R. Fan, V. Terzija, "Power System Restoration: a Literature Review from 2006 to 2016", *Journal of Modern Power Systems and Clean Energy* **4**(3), July 2016, p. 332-341.

[16] K. Sun, Y. Hou, W. Sun, J. Qi, Power System Control Under Cascading Failures, pub. IEEE Press 2019, ISBN 978-1-119-28202-0.

[17] J. Brombach, C. Hachmann, D. Lafferte, A. Klingman, W. Heckmann, F. Welck, D. Lohmeier, H. Becker, "The Future of Power System Restoration", *IEEE Power and Energy Magazine* Nov/Dec 2018, p. 30-41.

[18] M. Ropp, M. Reno, M. Biswal, "Detection and Prevention of Unintentional Formation of Loops in Self-Healing Power Systems and Microgrids", *IEEE Transactions on Power Delivery* (early access), March 15 2023.

[19] E. Silva, O. Lavrova, M. Ropp, "Protection Elements for Self-Healing Microgrids Using Only Local Measurements", Proceedings of the 2022 North American Power Symposium (NAPS), Oct 2022.

[20] M. Ropp, O. Lavrova, S. Ranade, A. Ramoko, C. Valdez, "Results of Late-Start LDRD Project 'SHAZAM'", Sandia National Laboratories report SAND2021-11593, available online at https://www.osti.gov/servlets/purl/1821319

[21] IEEE PES Test Feeder web site, https://cmte.ieee.org/pes-testfeeders/resources/.

[22] IEEE Std C37.2-2008, "IEEE Standard for Electrical Power System Device Function Numbers, Acronyms, and Contact Designations"